

Tetrabasic Lead Sulphate Micro-Rods as Positive Active Material for Lead Acid Battery

Zhenzhen Fan^{1,2}, Beibei Ma^{1,2}, Wei Liu^{1,2}, Fajun Li^{1,2}, Yanqing Zhou^{1,2}, Jian Tai^{1,2}, Xiaoyuan Zhao^{1,2}, Lixu Lei^{1,2,*}

¹ School of Chemistry and Chemical Engineering, Southeast University, Nanjing, 211189, China

² The Jiangsu Key Laboratory for Advanced Metallic Materials, Nanjing, 211189, China

*E-mail: lixu.lei@seu.edu.cn

Z.Z. Fan and B.B. Ma contributed equally to this work.

Received: 27 February 2018 / Accepted: 20 April 2018 / Published: 10 May 2018

It is well known that positive electrodes with high content of tetrabasic lead sulphate (4PbO·PbSO₄, short as 4BS) can improve the cycle performance of lead acid batteries (LABs). To achieve this, the positive plates are usually fabricated with addition of 4BS micro-crystals and long-time curing at high temperature, which is very costly. Herein, we report a fast and feasible route to produce 4BS, which are micro-rods of about 10 μm in length and 1 μm in diameter. In this article, we show a comparison of the electrochemical performances of the original as-prepared 4BS and pulverised 4BS crystals (dimensions of 0.5 to 2 μm) in positive electrodes. The original 4BS shows much better performances than the pulverised. The original discharges a capacity of more than 100 mAh g⁻¹ even after 1000 cycles of 100% DOD (depth of discharge) at 100 mA g⁻¹ in a flooded cell. Moreover, addition of 10% Pb₃O₄, 0.5% Sb₂O₃ and 0.5% SnSO₄ to the original 4BS increases the discharge capacity to 121.0 mAh g⁻¹. Therefore, we conclude that 4BS micro-rods can be directly used as the positive active material, which simplifies and unifies the production of LABs.

Keywords: Lead acid battery; tetrabasic lead sulphate; positive active material; cycle life; additive

1. INTRODUCTION

Lead acid batteries (LABs) have been widely used as mobile power sources for more than 150 years due to the advantages of abundant materials, high safety, high reliability, mature fabrication technology and low cost [1]. However, to meet the power demands of the electric vehicles, electric bicycle and uninterruptible power supply nowadays, lead acid batteries must be further improved in specific capacity and cycle life at high charge and discharge current densities. Recently, large scale

electric energy storage required by the erupting solar electricity is demanding uniformity of batteries, which also demands novel production route of LABs, because the quality of leady oxide and formation process is difficult to control.

It has been found in our lab that PbSO_4 can be used as the negative active material (NAM) of LABs with satisfying property [2], but it is not so satisfactory if it is used as the positive active material (PAM) [3]. Consequently, we tried other ways, including preparing the basic lead sulphates chemically, and using them as active materials directly. Since those materials can be produced with high uniformity, they could change the aspects of LAB production, and no leady powdering and curing process is needed anymore. Most importantly, those materials can be directly produced from spent LABs [4]. Here, we report what we have found on tetrabasic lead sulphate ($4\text{PbO}\cdot\text{PbSO}_4$, short as 4BS), which has been used as the PAM.

Previous studies have found that the cycle life can be efficiently improved if the proportion of 4BS is increased in the positive lead paste [5-8], because that kind of electrode has stable conductive framework, which can alleviate softening and shedding (the principal factor causing failure of LABs) of the positive electrode [8-10]. Up to now, there are two methods to manufacture the positive electrodes with high content of 4BS: (1) increasing the temperature during the mixing of lead paste and curing of the plate, because high temperature ($80 \sim 90 \text{ }^\circ\text{C}$) is needed for the formation of 4BS [7, 11-13]. For example, D. Pavlov et al. [7] prepared 4BS paste with a semi-suspension technology, and the dimensions of 4BS crystals after curing process at $90 \text{ }^\circ\text{C}$ are about $20 \sim 25 \text{ }\mu\text{m}$, which shows high capacity (about 90 mAh g^{-1} at 65 mA g^{-1}) and long cycle life (more than 200 cycles); (2) using small 4BS crystals as crystal seeds [10, 14]. For example, Lang et al. [10] reported that adding 4% of nanometre 4BS to the positive paste can effectively improve the cycle life of the battery. The discharge capacity at 0.5 C is about 68 mAh g^{-1} initially, and it is still higher than 60 mAh g^{-1} after 80 cycles; Boden et al. [14] used lead monoxide with addition of 1% 4BS (particle size of about $1 \text{ }\mu\text{m}$) to prepare lead paste with presence of 80% 4BS, but the battery performance was not declared.

Usually, the commercial curing process should be carried out between $70 \text{ }^\circ\text{C}$ and $90 \text{ }^\circ\text{C}$ for several days, because the oxidation of metallic lead in the leady oxide and formation of 4BS take time. Directly using 4BS as the raw materials for PAM can eliminate the traditional curing process and decrease the production cost of LABs [9, 15], if 4BS can be prepared at low cost. M. Cruz-Yusta et al. [9] prepared 4BS through hydrothermally method, and then sprayed it on a lead alloy substrate with a coating thickness of $100 \text{ }\mu\text{m}$. The obtained electrode delivered a capacity of 115 mAh g^{-1} with excellent capacity retention over 550 cycles at 100% depth of discharge (DOD). However, these results may be affected by the substrate lead alloy and the thin electrode (only $20 \text{ mg 4BS per cm}^2$). Biagetti and Weeks [15] synthesized 4BS with around $22 \text{ }\mu\text{m}$ in length and $3.5 \text{ }\mu\text{m}$ in diameter and used it directly as PAM, but the electrode discharged only 50 mAh g^{-1} at 41 mA g^{-1} , although a long time formation process of about 261 hours was taken. Torcheux et al. [5] suggested that reducing the crystal size of 4BS (especially the section) can improve the efficiency of formation process. Applying long 4BS crystal with a small section as positive material can greatly improve the interconnection degree, porosity and specific surface of the electrode. S. Grugeon-Dewaele et al. [16] studied the influence of the thickness of the 4BS needles on the capacities, which shows that thinner 4BS crystals ($< 3 \text{ }\mu\text{m}$) are better for the performance of the positive electrodes. Lang et al. [10] found that

nanometre 4BS as PAM can discharge a capacity of 175 mAh g^{-1} at 80 mA g^{-1} . However, they did not share the details of the electrode.

Recently, we have developed a fast and easy route to prepare 4BS at low cost, which is now being applied industrially. Here, we report a positive electrode made from an aqueous paste of pure 4BS with dimensions of $10 \mu\text{m}$ in length and $1 \mu\text{m}$ in diameter, which is pasted on ordinary lead alloy grid and used directly after drying, without curing process. Surprisingly, the positive electrode delivers high capacity and excellent cycle life at high charge and discharge current density of 100 mAh g^{-1} (mass of electrode less lead grid) and 100% DOD.

2. EXPERIMENTAL

2.1 Materials

$4\text{PbO}\cdot\text{PbSO}_4$ (4BS) was prepared in water from PbO and sulphuric acid in the molar ratio of 5:1. The reaction takes only 3 hours under ordinary conditions. Other materials are purchased and used without any further treatments.

2.2 Characterization

Powder X-ray diffraction patterns (XRD) were measured on a SHIMADZU XD-3A diffractometer (Japan) with Cu $K\alpha$ radiation, and the scan rate was $0.2^\circ \text{ min}^{-1}$ with 0.02° step. The morphologies of the samples were observed on a scanning electron microscope (SEM, FESEM FEI Inspect F50, USA) and a transmission electron microscopy (TEM, JEM-2100, Japan). The N_2 adsorption–desorption isotherms at 77 K were performed using a Quantachrome Nova 1200e surface area and porosity analyser (USA).

2.3. Electrode preparation

Short polyester (PET) fibre, graphite, commercial negative plate and absorptive glass-mat (AGM) membranes were provided by Huafu Energy Storage Co., Ltd.

A positive paste was made by mixing 1.0 g of 4BS, 0.003 g of short polyester fibre, 0.003 g of graphite and a certain amount of deionized water to meet the required density of the paste (4.0 g cm^{-3}), and then evenly applied onto a Pb-Ca alloy grid with dimensions of $10 \times 8 \times 2 \text{ mm}^3$. Subsequently, the plate was immersed into the sulphuric acid of 8 wt.% for 5 s and dried at 100°C for 5 min. Then, the plate was directly put into an oven maintained at 70°C for 24 h. The mass of the PAM was calculated by using the mass of the dried plate minus that of the blank grid.

Two electrodes were made according to the above procedure from both the original 4BS and pulverised 4BS made by grinding the original 4BS, which will be indicated as original 4BS electrode and pulverised 4BS electrode hereafter, respectively.

Several other positive plates were also made according to the above procedures, but more additives were used, such as Pb_3O_4 , Sb_2O_3 and SnSO_4 . Here, only the best of the formulation are reported, which is 10% Pb_3O_4 , 0.5% Sb_2O_3 and 0.5% SnSO_4 . The masses of 4BS, fibre and graphite are same as above.

2.4. Electrochemical performance test

The prepared positive plate was assembled with a commercial negative plate (dimensions of $10 \times 24 \times 2 \text{ mm}^3$) and absorptive glass-mat (AGM) as separator. Then, they were placed into a plastic case, in which a H_2SO_4 solution with a relative density of 1.26 g cm^{-3} was used as the electrolyte. After the assembled plates had been immersed in H_2SO_4 solution (1.26 g cm^{-3}) for 2 h, the battery formation process was started. All of the formation and the cycling tests were carried out with an NEWARE BTS-5V3A Cycler (China).

The formation process was achieved by three steps: firstly, the electrode was charged at a current density of 15 mA g^{-1} for 100 mAh g^{-1} ; secondly, it was charged at 25 mA g^{-1} for another 150 mAh g^{-1} ; finally, it was charged at 8 mA g^{-1} for 100 mAh g^{-1} . Since the capacity of commercial negative electrode is much larger than that of prepared positive electrode, the battery capacity was restricted by the as-prepared positive electrode.

After formation, the battery was discharged at 100 mA g^{-1} until the voltage fell to 1.75 V. Then it cycled according to the following procedure: firstly, it was charged at 100 mA g^{-1} until the battery voltage increased to 2.45 V; then it was charged at 50 mA g^{-1} for 60 mAh g^{-1} or the battery voltage increased to 2.84 V; finally, it was discharged at 100 mA g^{-1} until the voltage fell to 1.75 V.

After 50 cycles and rate tests, the positive electrode was disassembled from test battery and used as the work electrode for the cyclic voltammetry (CV) and electrochemical impedance spectroscopy (EIS) tests measured on the CorrTest CS350 electrochemical working station (China). To build a three-electrode system, a platinum foil and a saturated $\text{Hg}/\text{Hg}_2\text{SO}_4/\text{K}_2\text{SO}_4$ electrode were used as the counter and reference electrodes, respectively, and the electrolyte was 1.26 g cm^{-3} of H_2SO_4 solution. EIS measurements were carried out by applying an AC voltage amplitude of 5 mV in the frequency range from 10^{-1} Hz to 10^5 Hz at the potential of 1.1 V.

3. RESULTS AND DISCUSSION

3.1 The characterisation of the materials

Fig. 1 shows the XRD patterns of the original 4BS and the pulverised 4BS made by grinding the original. All of the peaks of the XRD patterns of the both 4BS samples can be readily indexed to a pure monoclinic phase (space group: $P2_1/c$) of 4BS with lattice constants $a = 7.315 \text{ \AA}$, $b = 11.713 \text{ \AA}$, and $c = 11.525 \text{ \AA}$ ($90.0 \times 90.956 \times 90.0$), which are very similar to the literature values (JCPDS 23-0333) of $a = 7.307 \text{ \AA}$, $b = 11.717 \text{ \AA}$, and $c = 11.532 \text{ \AA}$ ($90.0 \times 91.0 \times 90.0$). Therefore, grinding does not change the crystal structure of 4BS. Both of the samples have a series of sharp and intense peaks at

10.7°, 27.6°, 28.7°, 29.2°, 31.0° and 33.6°, corresponding to (110), ($\bar{2}$ 30), ($\bar{2}$ 02), (202), (400) and (032) faces of 4BS, respectively.

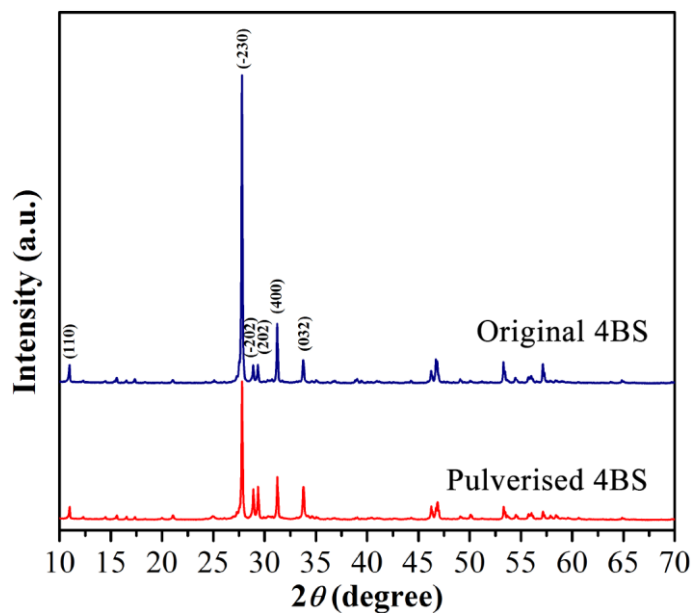


Figure 1. X-ray diffraction patterns of the original prepared 4BS and pulverised 4BS.

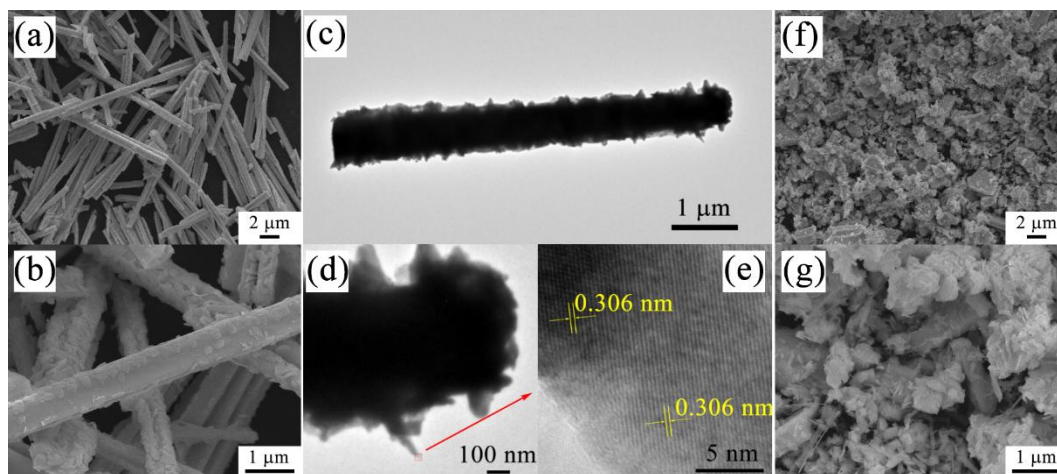


Figure 2. SEM images of (a, b) original prepared 4BS and (f, g) pulverised 4BS. Also the TEM images (c, d) and (e) HRTEM image of a 4BS micro-rod from the original prepared 4BS.

The scanning electron microscopy (SEM) images of the two 4BS samples are shown in Fig. 2. It can be seen that the original prepared 4BS are micro-rods with dimensions of about 10 μm in length and 1 μm in diameter. The high magnification SEM image (Fig. 2b) indicates that there are many scales with about 200 nm in dimension clung to the surface of the micro-rods. Fig. 2e displays a typical TEM image of an individual 4BS micro-rod with nano-scales on the surface. From the enlarged fraction (Fig. 2d), many nano-scales grows on the edge of the rod, which is consistent with SEM

images. The HRTEM observation of an individual scale in Fig. 2e shows that the inter-planar spacing is 0.306 nm, which corresponds to the (202) plane of monoclinic 4BS, indicating these nano-scales are also 4BS phase. Fig. 2f and 2g reveal that the pulverised 4BS sample is irregular particles with dimensions from 0.5 to 2 μm .

Fig. 3a shows the composition of the electrode peeled from the electrode after drying. Compared with the raw 4BS, their XRD patterns show that both samples contain $4\text{PbO}\cdot\text{PbSO}_4$, $3\text{PbO}\cdot\text{PbSO}_4$ (JCPDS 29-0781) and $\text{PbO}\cdot\text{PbSO}_4$ (JCPDS 76-1579), which means that 4BS reacted with H_2SO_4 after the electrode was immersed in sulphuric acid.

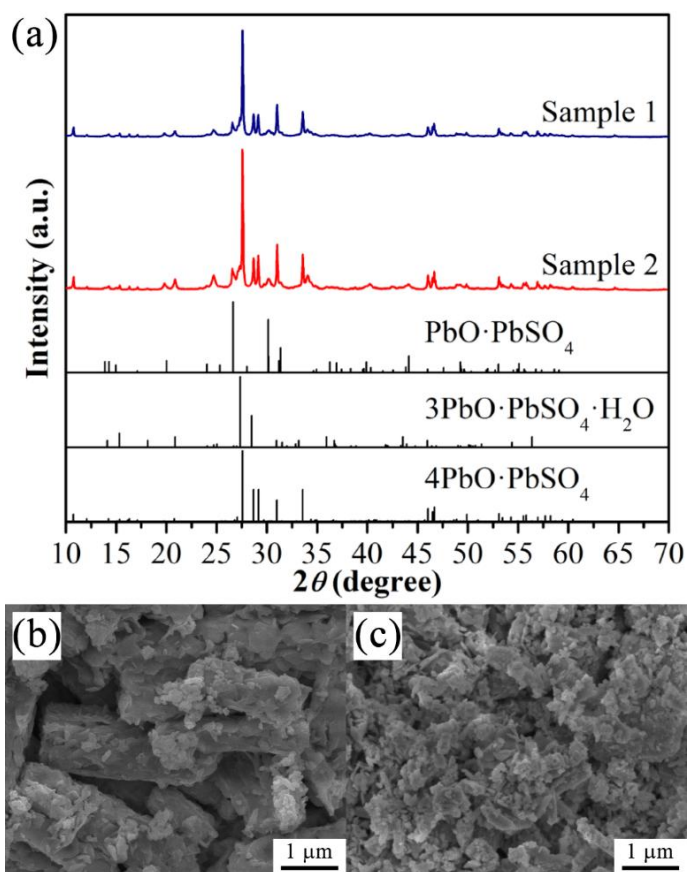


Figure 3. (a) XRD patterns and (b, c) FESEM micrographs of samples obtained from the original 4BS (sample 1) and the pulverised 4BS (sample 2) electrodes after drying.

3.2 The formation of the 4BS positive electrode

To detect the composition of the electrode after formation, the PAM was peeled from the electrode and ground for XRD analysis. Fig. 4a shows that both of the samples contain $\beta\text{-PbO}_2$ (JCPDS 76-0564) and PbSO_4 (JCPDS 82-1855); but the content of $\beta\text{-PbO}_2$ in the original 4BS electrode (sample 3) is 84.2 wt.%, which is much higher than that in the pulverised 4BS electrode (sample 4, 46.7 wt.%) as calculated with software Jade[®]. Therefore, the electrode used the original 4BS can be more easily formatted than the one used the pulverised 4BS.

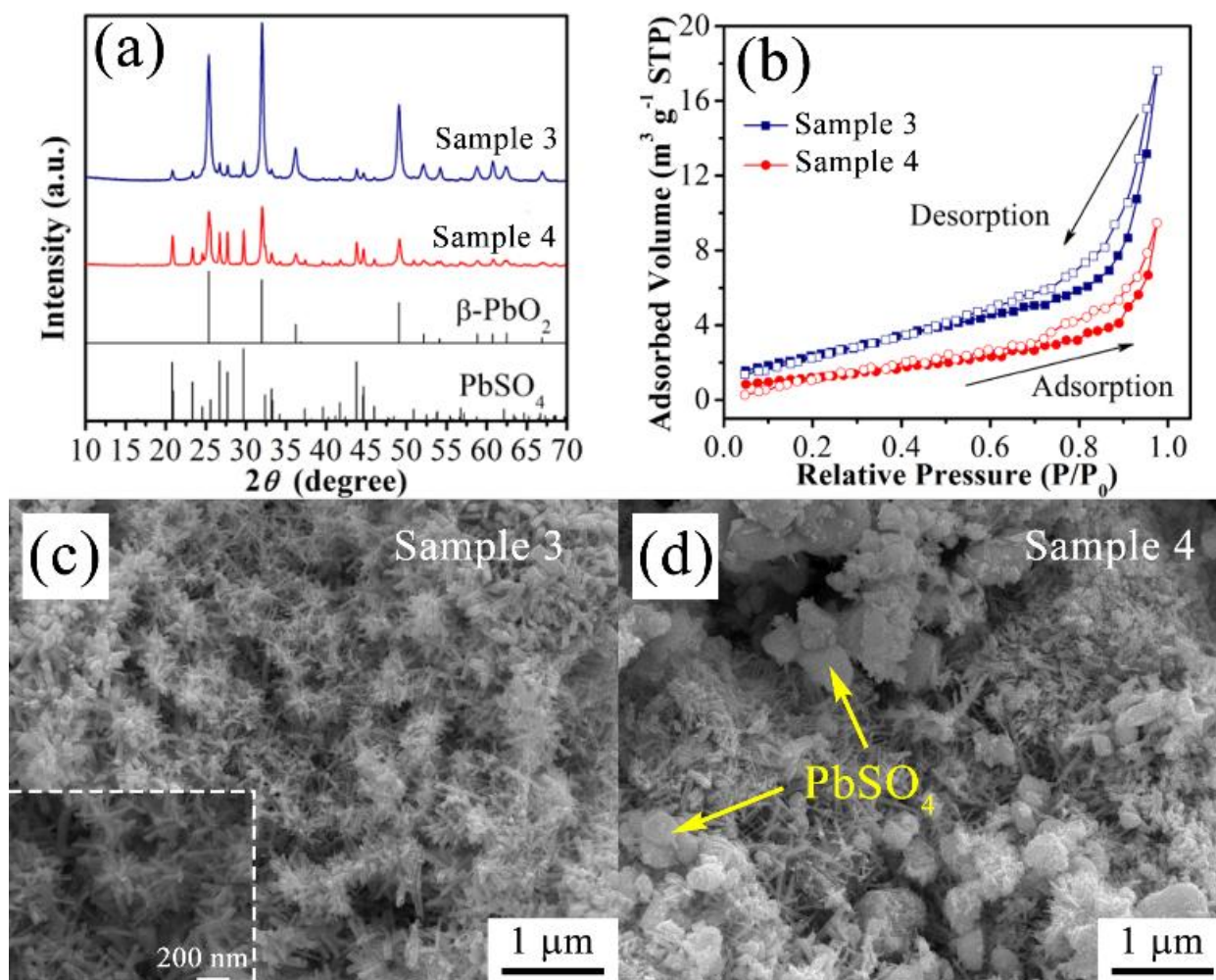


Figure 4. (a) XRD patterns, (b) N₂ adsorption–desorption isotherms and (c, d) FESEM micrographs of samples obtained from the original 4BS (sample 3) and the pulverised 4BS (sample 4) electrodes after formation.

Fig. 4c and 4d show the FESEM of electrode materials after formation. According to Fig. 4a, 4c and 4d, it can be seen that the original 4BS electrode has uniform PbO₂ nano-whiskers with about 30 ~ 80 nm in diameter and about 200 nm in length. However, for the pulverised 4BS electrode, apart from some agglomerated PbO₂ nano-whiskers, there are also a mass of PbSO₄ crystals, which is consistent with the higher content of PbSO₄ observed from the XRD analysis. The analysis of nitrogen adsorption-desorption isotherms of the samples (Fig. 4b) shows that Brunauer-Emmett-Teller (BET) specific surface areas of the samples from original 4BS and pulverised 4BS electrodes are 9.741 and 4.642 m² g⁻¹, respectively, and the larger surface area of the original 4BS electrode can provide more active sites for the electrochemistry reaction, leading to the better electrochemical performance than the pulverised 4BS electrode.

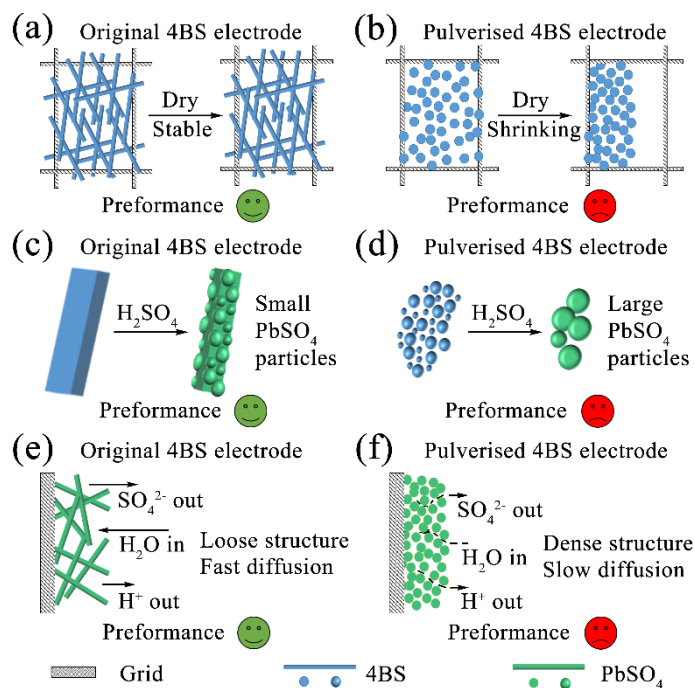


Figure 5. Schematic diagram of the differences between the two 4BS electrodes during (a, b) drying process, (c, d) soaking process and (e, f) formation process.

Previous researches show that the conversion of 4BS to PbO_2 undergoes two main progresses: in the soaking process, 4BS is converted gradually to $PbSO_4$ (reaction 1); in the formation process, $PbSO_4$ is oxidized to PbO_2 by the electrochemical reaction (2) [1, 17-19].



In the latter process, transportation of electrons and reaction species (H^+ , SO_4^{2-} and H_2O) from/to the reaction sites are required between PAM and electrolyte. Difficulties in the movement of these reaction species may regulate the conversion process [1, 19]. In the present study, as illustrated in Fig. 5, the difference (phase composition and morphology) between the original 4BS and pulverised 4BS electrodes after formation may be due to three main reasons: (1) the branchy long crystalline rods of 4BS used as PAM cause less shrinkage, and make tight electric connection to the grid frame (Fig. 5a), while the pulverised 4BS particles cause much more shrinkage (Fig. 5b), leading to part of PAM loss the connectivity to grid frame, resulting in the poor electrochemical properties [15]; (2) during the soaking and formation process, 4BS will react with H_2SO_4 to form $PbSO_4$. While the branchy large 4BS micro-rods have smaller specific surface area, the reaction may be a bit slower, and $PbSO_4$ particles are far apart from each other, thus the $PbSO_4$ particles are difficult to grow up (Fig. 5c); the pulverised 4BS electrode are just the opposite, which makes the $PbSO_4$ particles grow up easily and hard to convert to PbO_2 (Fig. 5d); (3) the steric hindrance of the original 4BS makes the electrode have a loose and porous microstructure, which is beneficial for the diffusion of reaction species (H^+ , SO_4^{2-} and H_2O) in and out of the electrode, and helpful to the conversion of $PbSO_4$ to PbO_2 , while the pulverised 4BS particles makes the electrode denser and reaction slower (Figs. 5f and 5e).

3.3 The electrochemical performance of original 4BS and pulverised 4BS electrodes.

Fig. 6a shows the cyclic performance of the original 4BS and pulverised 4BS electrodes at a discharge current density of 100 mA g^{-1} (1 C). The discharge capacities of the two kinds of electrodes are quite stable and gradually increasing during the first 50 charging and discharging cycles at 100% DOD. After 50 cycles, the discharge capacity of the original 4BS electrode is 97.4 mAh g^{-1} at 100 mA g^{-1} , which is nearly 2 times of the pulverised 4BS electrode (50.3 mAh g^{-1}). Therefore, too small particles are not good for high performance.

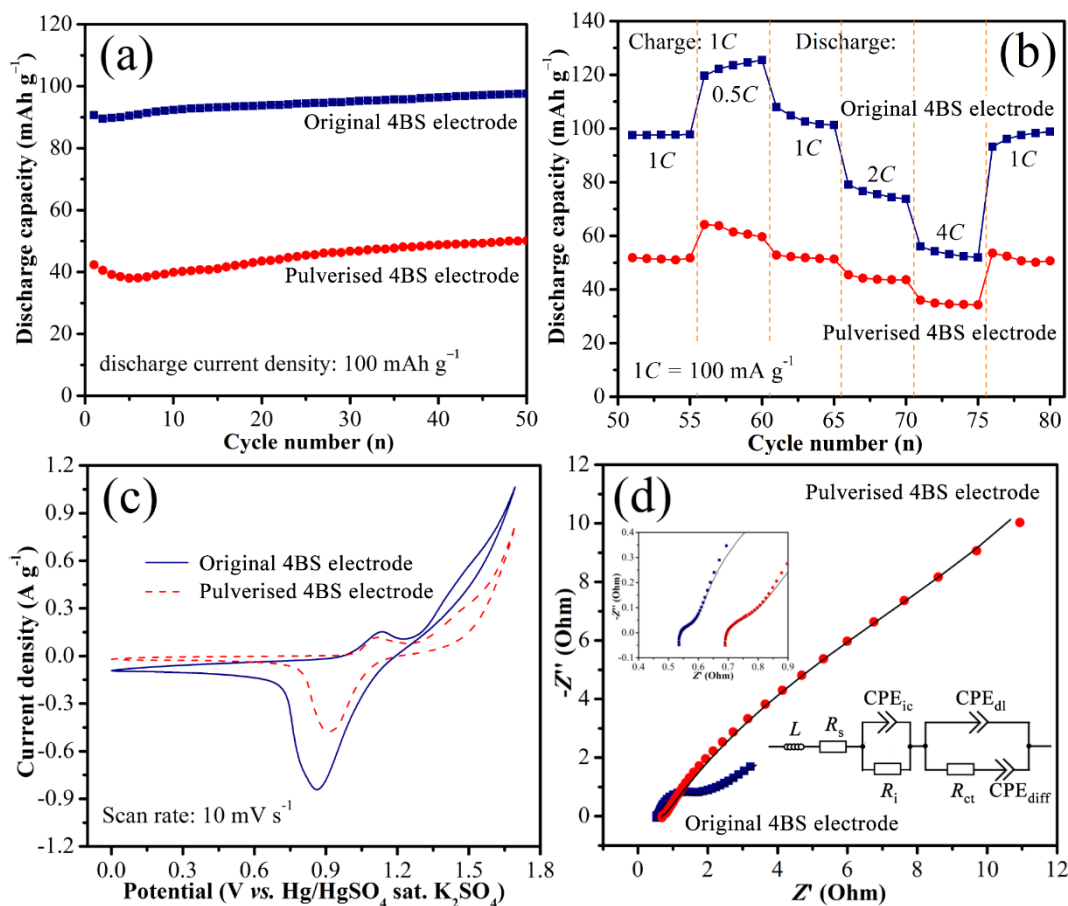


Figure 6. (a) The discharge capacity versus cycle number, (b) the capacities at different discharge rate, (c) Cyclic voltammety curves, and (d) Nyquist plots of original 4BS and pulverised 4BS electrodes.

Fig. 6b shows the influence of discharge current density on the discharge capacity after 50 cycles at 100% DOD. It can be seen that the discharge capacities of the original 4BS electrode are about 123.7, 97.3, 75.4 and 53.1 mAh g⁻¹ at discharge current density of 0.5 C, 1 C, 2 C and 4 C (1 C = 100 mA g⁻¹), respectively. The discharge capacity comes back to about 97 mAh g⁻¹ when the discharge current density is 1 C again, which indicates that the positive electrode use original 4BS as PAM are quite stable. Here, the utilization of active material is defined as the ratio of the discharge capacity and the corresponding theoretical capacity of 4BS, which is about 179.3 mAh g⁻¹. The

utilizations of the original 4BS electrode are about 69.0, 54.3, 42.1 and 29.6% at 0.5 C, 1 C, 2 C and 4 C, respectively. Similarly, the pulverised 4BS electrode also shows stable property in the discharge rate test, yet it is worse than the original 4BS.

Fig. 6c reveals the CV curves of original 4BS and pulverised 4BS electrodes after 50 cycles and rate tests measured between 0 V and 1.7 V (*vs.* Hg/Hg₂SO₄ in sat. K₂SO₄) at a scan rate of 10 mV s⁻¹. It can be seen that the oxidation of PbO to α -PbO₂ occurs at about 1.1 V, the oxidation of PbSO₄ to β -PbO₂ occurs at about 1.4 V, and the 0.9 V is attributed to the reduction of β -PbO₂ to PbSO₄ [1, 20]. Both of the two CV curves are similar, but the original 4BS electrode displays a higher current density than the pulverised 4BS electrode under the same conditions.

Electrochemical impedance spectroscopy (EIS) method was used to investigate electrochemical behaviour of the two electrodes at the potential of 1.1 V, which is the initial charge potential. Fig. 6d shows the Nyquist plot and the appropriate equivalent electrical circuit, which reflect the physical reality of the electrode [1, 20-22]. Here, inductive behaviour (L) at high frequencies is attributed to the interconnected structure together with connectors and external contributions. R_s is a serial resistance component at high frequencies which comes from intermediate layer, interfacial resistance and electrical connections. R_{ct} is the charge transfer resistance of the redox reaction on PAM and electrolyte interface. CPE_{diff} is a constant phase element representing the diffusion processes for SO₄²⁻ and H⁺ to the reaction layer. Because part of PbSO₄ is transformed to PbO₂, the pseudo-capacitance is high at PAM and electrolyte interface [23]. The constant phase element (CPE_{dl}) is introduced to replace the electric double layer capacitor. n denotes the deviation from the ideal behaviour, $n = 0$ for the pure resistors, $n = 0.5$ for the Warburg element and $n = 1$ for the perfect capacitors. At the beginning of the charge process, firstly, PbO_n and PbSO₄ in the interface of corrosion layer (CL) and the adjacent PAM layer (active mass connecting or collecting layer, AMCL) are oxidized, and then the PbSO₄ in PAM [23]. This is in good consistent with two oxide process observed in the CV curves (Fig. 6c). Consequently, an additional $CPE_{ic}R_i$ circuit appears at high frequencies. R_i is the ohmic resistance of the CL+AMCL interface, and CPE_{ic} is a constant-phase element representing the dielectric properties of the CL + AMCL layer.

Table 1. EIS simulation parameters of original 4BS and pulverised 4BS electrodes at 1.1 V in 1.26 g cm⁻³ H₂SO₄ solution at room temperature.

	Original 4BS	Pulverised 4BS
L (μ H)	0.691	0.717
R_s (Ω)	0.511	0.681
R_{ct} (Ω)	0.104	0.287
R_i (Ω)	0.743	2.205
CPE_{diff} ($\Omega^{-1} s^n$)	0.567	0.0842
n_1	0.65	0.72
CPE_{dl} ($\Omega^{-1} s^n$)	0.389	0.0620
n_2	0.35	0.53
CPE_{ic} ($\Omega^{-1} s^n$)	0.464	1.42
n_3	1.0	0.90
χ^2	8.17×10^{-3}	3.25×10^{-3}

The simulated data of electrochemical element mentioned above are listed in Table 1. It can be seen that R_s , R_{ct} and R_i of the original 4BS electrode are smaller than that of the pulverised, which means that the electrochemical performance of original 4BS electrode is much better than that of pulverised 4BS electrode. This is attributed to the loose and porous structure, and morphology of the original 4BS electrode (please refer to Fig. 4c). Firstly, the loose and porous structure of original 4BS electrode owns the lower pore resistance and contact resistance among PbO_2 particles than that of the compacted pulverised 4BS electrode; secondly, long 4BS micro-rods get stronger connection between PAM and grid than pulverised 4BS particles, which is beneficial for the electron transfer from grid to PAM.

3.4 The cyclic performance of the original 4BS electrode

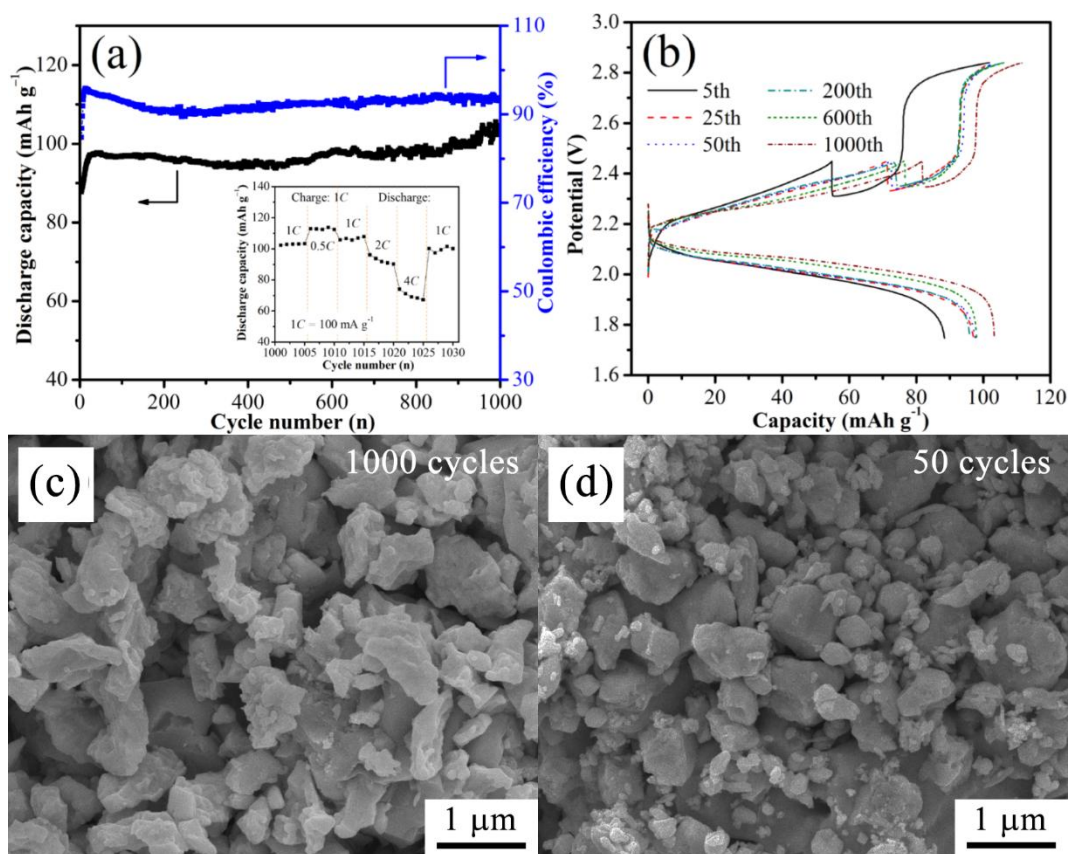


Figure 7. (a) The discharge capacity and coulombic efficiency *versus* cycle number for the original 4BS electrode, and the inset picture is the capacities at different discharge rate after 1000 cycles at 100% DOD; (b) the related curves of potential *versus* capacity at the 5th, 25th, 50th, 200th, 600th and 1000th cycles. SEM images for the discharged PAM scraped off original 4BS electrode after (c) 1000 and (d) 50 cycles.

Considering of the excellent electrochemical performance of the original 4BS electrode, the electrode was tested for 1000 100% DOD cycles at current density of 100 mA g^{-1} . As shown in Fig. 7a, the discharge capacity of the electrode increase from 87.8 mAh g^{-1} to 96.5 mAh g^{-1} in the initial 20 cycles and keeps stable at 97 mAh g^{-1} in the following 500 cycles. It is noteworthy that the discharge

capacity gradually rises to 103 mAh g^{-1} in the next 500 cycles, which is 117% of the initial capacity and 106% of the stable capacity. Moreover, the coulombic efficiency of the electrode is higher than 90% during the 1000 cycles, showing that the original 4BS electrode has the high cell efficiency. Therefore, the original 4BS electrode has an extraordinary cycle performance.

Fig. 7b reveals the changes of potential *versus* capacity during the different stages of 1000 charging and discharging cycles. It can be seen that in the first charging stage at 100 mA g^{-1} of the 5th cycle the battery potential rises to 2.45 V while the charged capacity is only 55 mAh g^{-1} . In the second charging stage at 50 mA g^{-1} , after about 20 mAh g^{-1} of capacity was charged, the battery potential increased rapidly to above 2.7 V, and another 20 mAh g^{-1} of capacity is added at high potential of 2.7 V. However, with the increasing of the cycle number, the charged capacity in the first charging stage is growing, indicating more energy can be charged into the battery at potentials lower than 2.45 V and the second charging stage becomes shorter. For the discharge process, the potentials become higher as the cycle number getting bigger. Hence, it can be concluded that the electrode becomes better and better with the increase of cycles.

After 1000 cycles, the battery was further tested for a rate performance. As shown in the inset of Fig. 7a, the discharged capacities of the original 4BS electrode after 1000 cycles are about 113.8, 103.3, 91.8 and 69.2 mAh g^{-1} at discharge current density of 0.5 C, 1 C, 2 C and 4 C (1 C = 100 mA g^{-1}), respectively. It is noteworthy that although the discharged capacities at 0.5 C is 8.0% lower than that of the electrode after 50 cycles, there are about 6.2%, 21.7% and 30.3% increase in the discharged capacities at 1 C, 2 C and 4 C, respectively.

The SEM images of discharged PAM scraped off original 4BS electrode after 1000 cycles and 50 cycles are shown in Fig. 7c and 7d, respectively. It can be seen that PbSO_4 particles are well dispersed with dimensions from 0.4 to $1 \mu\text{m}$, which is about the same as those in the electrode after 50 cycles. Thus we believe that it is the branchy nature of the original 4BS micro-rods that stops the PbSO_4 growing and make the electrode stable.

3.5 Addition of Pb_3O_4 , Sb_2O_3 and SnSO_4 on cyclic performance of original 4BS electrodes

It is known that Pb_3O_4 can promote the formation and deep-cycle performance [3]. Therefore, we added Pb_3O_4 into the electrodes to improve the performance of original 4BS electrode (Fig. 8a). When Pb_3O_4 of 5%, 10% and 20% mass of 4BS were added, after 50 cycles, the discharge capacities of the electrodes are 90.8, 98.4 and 90.3 mAh g^{-1} at a discharge current density of 1C, respectively. Addition of 10% Pb_3O_4 can improve the discharge capacity to a large extent, which is 5.8% higher than the one without Pb_3O_4 (93.0 mAh g^{-1}).

Sb_2O_3 was also added to the PAM on the base of 10% Pb_3O_4 . As shown in Fig. 8b, Sb_2O_3 can improve the performance of the electrode, and 0.5% Sb_2O_3 is the best, which discharges 114.2 mAh g^{-1} after 50 cycles, 16.1% higher than the one only with 10% Pb_3O_4 as the addition.

SnSO_4 can improve the performance of deep cycle batteries and prevent the irreversible sulphation [24]. Fig. 8c shows that SnSO_4 may reduce the discharge capacity initially, but its discharge capacity after stabilization is bigger. Therefore, another experiment was done with Pb_3O_4 , SnSO_4 and

Sb_2O_3 of 10%, 0.5% and 0.5% mass of 4BS respectively added to the PAM. From Fig. 8d we can see that discharge capacity is 121.0 mAh g^{-1} after 150 cycles, 31.4% higher than the 4BS electrode without them (93.0 mAh g^{-1}).

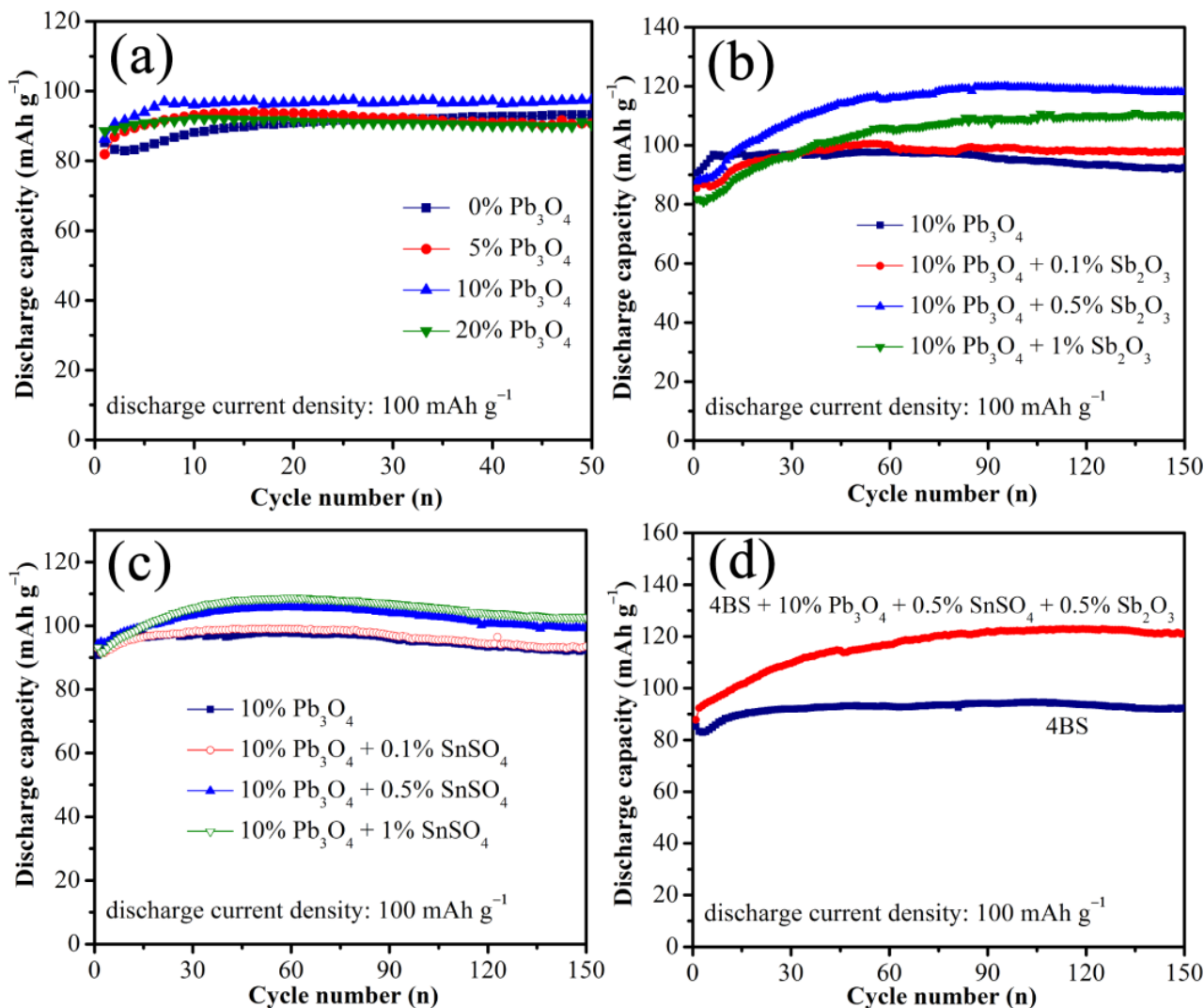


Figure 8. (a) The discharge capacities *versus* cycle number for the original 4BS electrodes with the addition of (a) Pb_3O_4 , (b) $\text{Pb}_3\text{O}_4 + \text{Sb}_2\text{O}_3$, (c) $\text{Pb}_3\text{O}_4 + \text{SnSO}_4$, and (d) $\text{Pb}_3\text{O}_4 + \text{Sb}_2\text{O}_3 + \text{SnSO}_4$, respectively.

In summary, we synthesized uniform 4BS micro-rods with 10 μm in length and 1 μm in diameter. When this material and additives is used as PAM for LABs, good electrochemical performances were obtained. Herein, we also make a comparison with the earlier reported materials as shown in the table 2.

Table 2 Comparison of the properties of different positive active materials for LABs.

Materials	Morphology	Current Collector	Discharge Current Density/ mA g^{-1}	Discharge Capacity/ mA h g^{-1}	Cycle Number	Reference
α -PbO	random particles	lead-coated glass fibre grid	22.5	120 ~ 140	50	[25]
α -PbO + β -lead	-----	Sn-Al-Ca-Pb alloy grid	50	65 ~ 160	50	[26]
PbSO ₄ + Pb ₃ O ₄	irregular flakes	Pb-Ca alloy grid	100	90 ~ 100	150	[3]
4BS	needle-shaped particles	SLI grid	65	90	≥ 200	[7]
4BS	needle-shaped particles	Pb-Ca-Sn alloy sheet	-----	115	≥ 550	[9]
4BS	rod-like particles	Pb-Ca alloy grid	41	50	-----	[15]
4BS	uniform rod-like particles	Pb-Ca alloy grid	100	87.8 ~ 103	1000	Our work
4BS+Pb ₃ O ₄ + SnSO ₄ + Sb ₂ O ₃	-----	Pb-Ca alloy grid	100	90~ 121	150	Our work

4. CONCLUSION

This paper demonstrated that uniform rod-like 4BS crystals with dimensions of 10 μm in length and 1 μm in diameter can be directly used as PAM for LABs. This means no curing process is needed, and manufacture cost can be saved.

Pulverisation of as-prepared 4BS crystals is no good for LABs, since more inert PbSO₄ is formed. The original 4BS electrode leads to higher β -PbO₂ content, larger BET surface area and uniform PbO₂ nano-whiskers after formation, which makes the electrode discharges a capacity of 103 mAh g^{-1} even after 1000 cycles of 100% DOD at 100 mA g^{-1} with above 90% of coulombic efficiency. The electrode can discharge about 70 mAh g^{-1} at a high rate of 4C (400 mA g^{-1}). We believe that it is the branchy nature of the 4BS micro-rods that makes the electrode stable, especially, PbSO₄ generated in the discharged process cannot grow up to big crystals.

Addition of Pb_3O_4 , SnSO_4 and Sb_2O_3 to the original 4BS electrode can further improve the performance of the electrode. When Pb_3O_4 , SnSO_4 and Sb_2O_3 of 10%, 0.5% and 0.5% mass of 4BS respectively added to the PAM, the discharge capacity of the electrode increases up to 121.0 mAh g^{-1} .

ACKNOWLEDGEMENTS

This work is partly supported by the Fundamental Research Funds for the Central Universities (3207047452), the Priority Academic Program Development of Jiangsu Higher Education Institutions and the Jiangsu Key Laboratory for Advanced Metallic Materials (BM2007204).

References

1. W. Liu, B.B. Ma, F.J. Li, Y. Fu, J. Tai, Y.Q. Zhou, L.X. Lei, *RSC Adv*, 6 (2016) 108513.
2. Y. Liu, P. Gao, X. Bu, G. Kuang, W. Liu, L. Lei, *J. Power Sources*, 263 (2014) 1.
3. K. Zhang, W. Liu, B. Ma, M.A. Mezaal, G. Li, R. Zhang, L. Lei, *J. Solid State Electrochem.*, 20 (2016) 2267.
4. L. Lei, B. Ma, J. Tai, Y. Zhou, W. Liu, CN106711531, (2017).
5. L. Torcheux, J.P. Vaurijoux, A. de Guibert, *J. Power Sources*, 64 (1997) 81.
6. S. Grugeon-Dewaele, S. Laruelle, F. Joliveau-Vallat, L. Torcheux, A. Delahaye-Vidal, *J. Power Sources*, 72 (1998) 126.
7. D. Pavlov, S. Ruvski, *J. Power Sources*, 95 (2001) 191.
8. D. Pavlov, *J. Power Sources*, 46 (1993) 171.
9. M. Cruz-Yusta, J. Morales, L. Sanchez, *J. Power Sources*, 157 (2006) 579.
10. X.S. Lang, D.L. Wang, C.Y. Hu, S.Z. Tang, J.S. Zhu, C.F. Guo, *J. Power Sources*, 270 (2014) 9.
11. D. Pavlov, N. Kapkov, *J. Electrochem. Soc.*, 137 (1990) 21.
12. D. Pavlov, M. Dimitrov, T. Rogachev, L. Bogdanova, *J. Power Sources*, 114 (2003) 137.
13. D. Pavlov, E. Bashtavelova, *J. Electrochem. Soc.*, 131 (1984) 1468.
14. D.P. Boden, D. Loosemo, *J. Power Sources*, 168 (2007) 90.
15. R.V. Biagetti, M.C. Weeks, *Bell System Technical Journal*, 49 (1970) 1305.
16. S. Grugeon-Dewaele, S. Laruelle, L. Torcheux, J.M. Tarascon, A. Delahaye-Vidal, *J. Electrochem. Soc.*, 145 (1998) 3358.
17. L.T. Lam, H. Ozgun, L.M.D. Cranswick, D.A.J. Rand, *J. Power Sources*, 42 (1993) 55.
18. M. Dimitrov, D. Pavlov, *J. Power Sources*, 93 (2001) 234.
19. D. Pavlov, N. Kapkov, *J. Electrochem. Soc.*, 137 (1990) 16.
20. T. Chen, H. Huang, H.Y. Ma, D.L. Kong, *Electrochim. Acta*, 88 (2013) 79.
21. D. Pavlov, G. Petkova, *J. Electrochem. Soc.*, 149 (2002) A654.
22. R.D. Marco, A. Lowe, M. Sercombe, P. Singh, *Electrochim. Acta*, 51 (2006) 2088.
23. W.L. Zhang, H.B. Lin, H.S. Kong, H.Y. Lu, Z. Yang, T.T. Liu, *Electrochim. Acta*, 139 (2014) 209.
24. Q. Wang, J. Liu, D. Yang, X. Yuan, L. Li, X. Zhu, W. Zhang, Y. Hu, X. Sun, S. Liang, J. Hu, R.V. Kumar, J. Yang, *J. Power Sources*, 285 (2015) 485
25. J. Wang, S. Zhong, G.X. Wang, D.H. Bradhurst, M. Ionescu, H.K. Liu, S.K. Dou, *Journal of Alloys and Compounds*, 327 (2001) 141.
26. C. Ma, Y.H. Shu, H.Y. Chen, *RSC Adv*, 5 (2015) 94895.